Direct determination of the self-diffusion mechanism in bcc β-titanium

G. Vogl
Institut für Festkörperphysik der Universität Wien, A-1090 Wien, Austria

W. Petry
Institut Max von Laue–Paul Langevin, Boîte Postale 156X, F-38042 Grenoble CEDEX, France

Th. Flottmann* and A. Heiming
Freie Universität Berlin, D-1000 Berlin 33, Federal Republic of Germany
and Institut Max von Laue–Paul Langevin, Boîte Postale 156X, F-38042 Grenoble CEDEX, France
(Received 12 October 1988)

With quasielastic neutron scattering the elementary diffusion jump (length and direction) and the jump frequency in bcc β-Ti single crystals have been determined at temperatures between 1460 and 1580 °C. Supplementary measurements on polycrystalline samples extended the temperature region down to 1100 °C. The elementary diffusion jump is a jump into a nearest-neighbor vacancy. An admixture of 10–15 % jumps into next-nearest-neighbor vacancies is compatible with the experiments. Comparison of derived diffusivities with results from tracer measurements shows satisfactory agreement.

I. INTRODUCTION

Self-diffusion in the bcc high-temperature phase (β phase) of the group-IV*b* (new IUPAC notation: Group-4) metals Ti, Zr, and Hf is anomalous in two respects (see, e.g., Herzig and Köhler[1]). (i) When plotted versus a normalized temperature T_m/T (where T_m is the melting temperature) the diffusivities are orders of magnitude higher than those of the other bcc metals. (ii) The Arrhenius plots are strongly curved, whereas for "normal" bcc metals the logarithm of the diffusivity deviates only slightly from a linear dependence on the reciprocal temperature.

Numerous attempts have been made during the past twenty years to explain anomalies in the diffusion of the bcc metals and in particular of the group-IV*b* metals. One group of explanations relies on the hypothesis that with *increasing temperatures* a second diffusion mechanism based on a second defect type gains increasing importance, suppressing progressively the diffusion mechanism via nearest-neighbor (NN) vacancies, which dominates at lower temperatures. For the second mechanism various explanations have been proposed: diffusion via divacancies,[2] next-nearest-neighbor (NNN) jumps,[3,4] or diffusion via interstitial sites.[5,6] Extensive studies by Herzig *et al.*[1] have proven that the earlier hypothesis of dislocations being responsible for a low-temperature enhancement of diffusion can be excluded.

Another group of explanations is based on the tendency of the group-IV*b* metals to undergo phase transitions. Already in 1967 Aaronson and Shewmon[7] suggested that the bcc lattice might destabilize when approaching the β-α (bcc-hcp) phase transition from above, leading to an enhancement of the diffusivity *with decreasing temperatures* relative to a normal Arrhenius-like behavior. Sanchez and DeFontaine[8] directed the attention to another phase transition, namely, to the low-temperature ω phase (hexagonal) which is suppressed in pure group-IV*b* metals under normal conditions, but occurs upon alloying and under pressure. Sanchez and DeFontaine suggested that in pure group-IV*b* metals a tendency to form activated complexes ("embryos") of the ω phase remains, this tendency being higher, the lower the temperature. Since the ω activated complexes should be produced by a freezing of soft longitudinal $\langle 111 \rangle$ phonons, the tendency to form ω activated complexes should go along with an increased number of NN jumps which are jumps in the $\langle 111 \rangle$ direction. Again this would lead to a relative increase of the diffusivity with decreasing temperatures. Recently Köhler and Herzig[9] revisited the controversy showing up the systematics of the anomalies in the bcc metals. They pointed out the correspondence between the change in the *d*-electron concentration and the tendency for phonon softening with the variation in the diffusivities and found a remarkable correlation between the activation energy for self-diffusion in bcc metals and the soft LA $\frac{2}{3}(111)$ phonon mode.[1,9]

A problem with all the diffusion models has been that no direct experimental evidence on a *microscopic* scale for one or the other explanation existed. All conclusions were drawn from tracer diffusion measurements, i.e., measuring penetration profiles of diffusing atoms, this method being a *macroscopic* one in that it studies the atomic distribution after a great number of jumps and thus averages over the elementary jump processes which, however, occur on an atomic (microscopic) scale. Conclusions on the elementary diffusion mechanism were possible through the development of sophisticated variants of the tracer techniques, i.e., by comparing the diffusivity of various isotopes (isotope effect) or studying the diffusivity after adding different solute concentrations. For instance, in the case of β-Zr it has been con-

cluded that the curvature in the Arrhenius plot can best be explained by a monovacancy mechanism with a temperature-dependent activation energy.[10] Nevertheless, tracer diffusion technique remains an indirect method for concluding on the elementary diffusion jump itself, because its basis are macroscopic quantities. This is certainly the main reason why for 20 years all the models could persist aside each other as possible explanations for the anomalous diffusion of the group-IV*b* metals, none of them sufficiently convincing to defeat the others.

Here, on the contrary, we shall present a direct atomistic determination of the elementary diffusion jump. First results have been published in a Letter.[11] A survey of the virtues of the nuclear methods in offering a microscopic picture of the dynamics of diffusion in metals has been given by Petry and Vogl.[12]

II. METHOD AND EXPERIMENTS

We shall first describe the way in which the diffusion mechanism can be determined from measurements of incoherent quasielastic neutron scattering; for further details we refer to the literature.[13] We shall then point out the special problems connected with studying in particular self-diffusion in β-Ti.

A. Incoherent quasielastic neutron scattering

The fate of an individual nucleus, and thus of an individual atom to which the nucleus belongs, is described by the incoherent part of the scattering intensity.[13] Contrary to coherent scattering there is no interference between neutron waves scattered at different atoms, i.e., no Bragg reflections appear. If, however, an atom during the scattering event jumps from one lattice site to another one, i.e., during the time the neutron interacts with the atom, then a phase shift will occur between the parts of the wave train scattered by the atom when at one site and when at the other site. Singwi and Sjölander[14] and—in a slightly different way—Chudley and Elliot[15] have derived the relation of jump frequency and jump vector (constituted by jump length and direction) with the energy change of the neutron: An energy broadening Γ of Lorentzian shape is superimposed on the incoherent elastic scattering which, because of its smallness, is called quasielastic broadening, the whole phenomenon being named quasielastic scattering (QNS). According to Singwi and Sjölander, for jumps between geometrically equivalent sites in a crystal ("long-range diffusion") the incoherent scattering function $S_{\rm inc}(\mathbf{Q},\omega)$ consists of one Lorentzian line centered around zero energy transfer,

$$S_{\rm inc}(\mathbf{Q},\omega)=\exp(-2W)\frac{1}{\pi}\frac{\Gamma(\mathbf{Q})/2}{[\Gamma(\mathbf{Q})/2]^2+(\hbar\omega)^2} \tag{1}$$

where the scattering vector $\mathbf{Q}=\mathbf{k}_f-\mathbf{k}_i$ is the difference between final and incident neutron wave vectors, $\hbar\mathbf{Q}$ being the momentum transfer to the scattered neutron, $\hbar\omega$ is the energy transfer, and $\exp(-2W)$ is the Debye-Waller factor. The width Γ (FWHM) of the quasielastic Lorentzian, i.e., the broadening with respect to the resolution function of the spectrometer ("quasielastic line broadening") depends on $\mathbf{Q}$ and on the atomic jump frequency and jump geometry. Please note that for jumps which scan a restricted region in space ("cage diffusion"), instead of one broadened Lorentzian several Lorentzians appear.[13,16,17] Then one of the lines remains narrow; the others, the number of which depends on cage symmetry, show different quasielastic broadening. The phenomenon of cage diffusion will not be of interest in this work.

For long-range diffusion which alone will be discussed here, and for random jumps of the atom to its N nearest neighbors, one obtains

$$\Gamma(\mathbf{Q})=\frac{2\hbar}{\tau}\left[1-\frac{1}{N}\sum_{n=1}^{N}\exp(i\mathbf{Q}\cdot\mathbf{R}_n)\right], \tag{2}$$

where $1/\tau$ is the jump frequency, τ being the time between the two jumps, and $\mathbf{R}_n$ are the $n=1,2,\ldots,N$ different possibilities for a jump vector leading from a given crystal position to a NN position. $\sum_{n=1}^{N}\exp(i\mathbf{Q}\cdot\mathbf{R}_n)$ has the analytical form of a structure factor, but what it determines is *not the intensity* of interferences but the *energy width* of incoherent scattering in reciprocal space. We term it the "width structure factor," which describes the matching of the phases of the neutron wave scattered at the different sites which the jumping atom occupies during the scattering process.

Since we want to apply QNS to decide between different competing models for the elementary diffusion jump we have to ask where these models enter into Eqs. (1) and (2). It is evident that it is $\mathbf{R}_n$ which has to be considered. We have therefore calculated the width structure factor for the different models discussed competitively in the literature.

1. *Diffusion via vacancies*

It is well known that the atomic jumps via vacancies in a crystal lattice do not constitute a random walk but are correlated, i.e., jumps back into a position where the atom has just come from are more probable than other jumps. The so-called encounter model takes into account both spatial and temporal correlation.[18] An encounter is defined as the sum of all displacements of a given atom caused by one and the same point defect. During one encounter some atoms may be displaced by more than the NN distance with a small but finite probability. In the encounter model, for the line broadening only the jump vector between original and final site is relevant, everything which happens in between is forgotten. Equation (2) modifies to

$$\Gamma(\mathbf{Q})=\frac{2\hbar}{\tau z_{\rm enc}}\left[1-\sum_{n}W_n\exp(i\mathbf{Q}\cdot\mathbf{R}_n)\right], \tag{3}$$

where $z_{\rm enc}$ is the average number of jumps of an atom during an encounter and W_n is the normalized probability that after the end of the encounter the scattering atom is displaced by a vector $\mathbf{R}_n$ (not necessarily a vector to a NN position). Both $z_{\rm enc}$ and W_n can be evaluated on the computer by simulating numerically a great number of encounters.[18] We have performed calculations for jumps

into nearest neighbors and into next-nearest neighbors both by making use of the encounter model.

2. *Diffusion on interstitial sites*

Quasielastic line broadening due to jumps on octahedral and tetrahedral interstitial sites in the bcc lattice was treated by Rowe *et al.*[19] long ago for the case of hydrogen diffusion on the basis of the line indicated by Chudley and Elliott.[15] The task which has already been solved by Rowe *et al.* is to set up the jump matrix describing the possible jumps between the sites considered for the special diffusion problem. Jumps on octahedral or tetrahedral interstitial sites show no correlation—the interstitial lattice is considered as an "empty lattice." Since the interstitial sites do not form a Bravais lattice, the m inequivalent sites ($m=3$ and 6 for octahedral and tetrahedral sites, respectively) give rise to m Lorentzians with different line broadenings Γ_m. For simplicity the different Γ_m have been averaged to *one* effective line broadening. We have set up a computer program which calculates the broadening Γ for a given jump mechanism, crystal orientation, and transferred momentum. We have considered jumps between nearest-neighbor sites only as it was done by Rowe *et al.*

For comparison with the experimental data the Lorentzian had to be folded with the experimental energy resolution (important correction) and with the Q resolution of the QNS spectrometer (minor correction).

B. Sample

1. *Choice of materials*

Out of the three group-IV*b* metals we have chosen titanium because its incoherent scattering cross section is one of the highest of all natural isotope mixtures: $\sigma_{\text{inc}}=2.7$ b.[20] Perturbation of the results by coherent scattering contributions is prevented through choosing a neutron wavelength $\lambda=6.28$ Å beyond the limit for the excitation of Bragg scattering.

2. *Crystal growth and characterization*

Titanium was purchased from MRC, France. The analysis provided by the manufacturer is the following: Al, 15; Cr, 20; Fe, 50; Ni, 30; Pb, 15; Sn, 20; Zr, <10; C, 30; H, 2; N, 4; O, 340 (wt. ppm). An additional analysis on the oxygen and nitrogen content performed by Bundesanstalt für Materialprüfung (BAM), Berlin, confirmed our suspicion regarding the low gas content as claimed by MRC. The BAM analysis on the basis of the hot-extraction method as standardized by the European Community gave N, 97(7) wt. ppm and O, 547(23) wt. ppm.

The martensitic phase transition from hcp α-Ti to bcc β-Ti at 882 °C makes it very difficult to perform experiments with β-Ti single crystals, the crystals being destroyed immediately once they are cooled below the transition temperature. We therefore have constructed a combined furnace for crystal growth and neutron scattering permitting to grow crystals by the zone melting technique in their high-temperature phase *in situ* on a neutron spectrometer. Without letting the crystal cool down below its transition temperature it can be oriented and a neutron scattering experiment can be performed. The furnace has recently been described by Flottmann *et al.*[21]

To optimize data statistics, large single-crystal samples are desirable. Our samples were each grown from a polycrystalline cylindrical rod of titanium metal, length 100 mm, diameter 8 mm. The rod was fixed between molybdenum metal clamps in vertical position. An alternating current of up to 600 A was passed through the sample; this "basic heating" permitting to keep the sample at any desired temperature up to T_m. By means of a circular electron gun a narrow zone of the crystal was molten. Crystals were grown by moving the electron gun, i.e., the molten zone with a typical velocity of 6 mm/h from bottom to top, over the sample. The absence of a heating element effects that neutron scattering comes nearly exclusively from the crystal, the furnace walls made of Al, and the Nb heat shields being very weak scatterers and in sufficient distance from the crystal. The sample environment was high vacuum (10^{-6} mbar during zone melting, $\leq 10^{-7}$ mbar afterwards). During crystal growth as well as afterwards (during the measurements), the temperature of the sample was controlled with a two-color pyrometer within ± 10 °C. A temperature gradient of $\pm 1\%$ within the 3-cm height of the neutron beam proved inevitable. We obtained single crystals of 3 to 5 cm length, their orientation being arbitrary since oriented seeds of the β phase (high-temperature phase) are principally not available.

The crystal orientation was directly determined on the backscattering spectrometer IN10 of the Institut-Laue-Langevin (ILL) by searching for the angular positions of the strong $\{110\}$ Bragg reflections. For this purpose we changed the incident neutron wavelength of IN10 to $\lambda=2.38$ Å by using the instrument's graphite reflector in direct reflection geometry. All these procedures have to be done without cooling the sample below 882 °C in order not to destroy the crystal. Figure 1 and the corresponding figure caption give the orientations of the crystals with respect to the scattering plane as they were found for the two QNS experiments. Due to the limited space in a backscattering spectrometer the only way to vary the orientation of a given crystal is to turn it around its vertical axis, which corresponds to the axis perpendicular to the scattering plane (z axis in Fig. 1). This variation in the scattering plane is denoted by the angle α, where α measures the angle in the scattering plane between the crystal $\langle 001 \rangle$ axis and the incident neutron wave vector $\mathbf{k}_i$ (x axis in Fig. 1). It happened that the scattering planes for crystal 1 and crystal 2 were close to $\{100\}$ and $\{210\}$ planes, respectively. The quality of the crystals was verified in test runs on a γ diffractometer: the mosaic spread of every as-grown crystal was always smaller than the instrumental resolution of 0.2°.

To complete the single-crystal measurements towards lower temperatures and, in particular, to perform measurements on the spin echo spectrometer, a few measurements on polycrystalline samples have been performed. For that purpose rectangular slices of $6\times30\times30$ mm

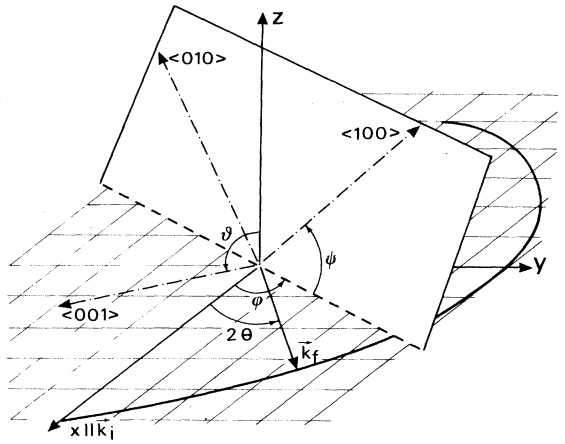

FIG. 1. Scheme of the crystal orientation with respect to the laboratory x,y,z frame as defined by the backscattering spectrometer IN10. The incident neutron wave vector $\mathbf{k}_i$ is parallel to the x axis and the direction of the scattered wave vector $\mathbf{k}_f$ varies within the x,y plane according to the analyzer positions with 2 times the scattering vector θ. The crystal's orientation can be defined by the three Euler angles: rotation φ, nutation ϑ, and precession ψ with signs defined by the arrows. The Euler angles (φ,ϑ,ψ) for crystals 1 and 2 were $(0°,0°,0°)$ and $(6.3°,22.1°,-4.2°)$, respectively. Crystal 1 had a $\{100\}$ scattering plane, crystal 2 had approximately a $\{210\}$ scattering plane.

were cut from the polycrystalline MRC material. To minimize contamination by gaseous impurities during the measurements each sample has been welded by an electron gun into a vacuum tight cylindrical Nb container with a wall thickness of 0.5 mm.

C. Measurements on single crystals

We have recently described in detail the measuring procedure for studying QNS of diffusion in metals for the case of fast impurity diffusion of Co in polycrystalline Zr–2 at. % Co;[22] here we therefore only discuss what is different for the case of self-diffusion in β-Ti and in particular for an *in situ* single-crystal growth.

From self-diffusivities measured by the tracer technique[23–26] one can estimate that temperatures rather close to the melting point of Ti (1675 °C) are necessary to obtain quasielastic line broadening of the order of the instrumental line width of the (ILL) backscattering spectrometer IN10 (set to FWHM $\simeq 1$ μeV in our case). We chose temperatures between 1460 and 1580 °C.

The total measuring time for each of the two crystals was 12 d at the IN10. To obtain maximum information on the diffusion-jump vector $\mathbf{R}_n$, four and three different orientations of crystals 1 and 2, respectively, were chosen consecutively. These orientations were realized by turning the whole furnace around its vertical axis, thus leaving the vertical crystal axis ([100] and [210], respectively) fixed, but changing the angle α of the $\langle 001 \rangle$ axis relative to the incident neutron beam in the scattering plane. Crystal 1 was measured at 1460 °C, crystal 2 was studied at 1465, 1530, and 1580 °C.

D. Measurements on polycrystalline samples

1. Backscattering measurements

Measuring on polycrystalline samples the orientational information is lost. The quasielastic line broadening is a function of the product of $|\mathbf{Q}|=Q$ with the elementary jump length d and a function of the jump frequency $1/\tau$:[22]

$$\Gamma(Q)=\frac{2\hbar}{\tau}\left[1-\frac{\sin(Qd)}{Qd}\right]f_{\text{nucl}} . \tag{4}$$

The linewidth is reduced by the correlation factor f_{nucl} which is slightly smaller than the tracer correlation factor f_{tr}.[18] Both factors take into account the directional correlation between successive jumps, i.e., the fact that a jump may be followed by a jump back into the original position. Measurements at $T=1410$, 1470, 1490, 1540, 1590 °C and for different Q have been performed on the backscattering spectrometer IN10.

2. Spin echo measurements

In order to have access to lower jump frequencies or smaller diffusivities it is necessary to measure the quasielastic line broadening with a better energy resolution. In principle the backscattering spectrometer IN10 can be operated with polished Si$\{111\}$ monochromator and analysers yielding a typical energy resolution of 0.3 μeV (FWHM). However, this gain in energy resolution with respect to the standard setup (1 μeV) has to be paid for by a loss in counting rate in the detector by a factor of 16. This leads to hopelessly long measuring times.

This situation can be overcome by measuring the jump frequencies by means of the spin echo spectrometer IN11 of the ILL.[27] This instrument accepts a large bandwidth $\Delta\lambda/\lambda$ of $\sim 10\%$ for the incoming neutrons with an energy resolution comparable and better than that of IN10. Different from the backscattering spectrometer, one measures the intermediate scattering law $S(Q,t)\propto e^{-t/\tau_{\text{SE}}}$, with the spin echo technique, i.e., direct a decay in time τ_{SE} without making use of the Fourier transform from time to energy. The decay in time can be converted to energy via the uncertainty relation. For an exponential decay it holds

$$\Gamma(\text{FWHM})=\frac{2\hbar}{\tau_{\text{SE}}} . \tag{5}$$

Due to the use of spin-polarized neutrons the technique is best suited for a coherent scatterer (no spin flip at the sample) and less appropriate for spin incoherent scatterers. Fortunately this argument does not hold for incoherent scattering from Ti. Ti with its natural isotope abundance is a so-called isotope incoherent scatterer with 87.2% fraction of zero spin scatterer, i.e., the incoherent scattering is dominated by the difference in scattering length of the three zero spin isotopes. Consequently, spin flip at the sample is of minor importance. To avoid uncontrolled neutron spin precession, particular attention has been paid to an almost magnetic field free heating system of the sample. Measurements at two tempera-

tures, 1165 and 1100 °C, respectively, and fixed $Q = 1.0$ Å^{-1} with an incident wavelength of 6.4 Å have been performed.

III. RESULTS FROM THE QNS MEASUREMENTS

A. Single crystals

Figure 2 shows a typical neutron spectrum obtained at the backscattering spectrometer IN10 with a single crystal at 1530 °C. All spectra could be well fitted by the convolution of the instrumental resolution function with one Lorentzian line.

Figure 3 shows for both crystals and two temperatures the linewidth $\Gamma(\mathbf{Q})$ (FWHM) for the different orientations (see Sec. II B) of the crystals relative to the incident beam at IN10. The error bars indicate the statistical errors.

Included in Fig. 3 are fits with expectations from various models discussed competitively in the literature. Figure 4 shows schematically the various models. Figure 4 also illustrates that an effective NNN jump cannot only be achieved by direct jumps into a NNN vacancy but also via a divacancy or by a three-dimensional dumbbell migration. The various models have been fitted simultaneously to all crystal orientations, thus leaving only *one* fit parameter τ for each of the two different temperatures. The resulting jump frequency $1/\tau$ is listed in Table I. Furthermore, Table I gives the values of χ^2, the quality-of-fit parameter, for optimum fits of the various models to the data. It is immediately evident from the figure and from the table that interstitial mechanisms are completely at variance with the experimental data. Thus diffusion via interstitial sites *alone* can be immediately excluded as the dominating diffusion mechanism. The same holds for dominating NNN jumps achieved by the mechanisms indicated in Fig. 4(b). However, the **Q** dependence of the diffusional line broadening can be well described by $\frac{1}{2}[111]$ jumps into NN vacancies. Please remember that for the NN vacancy mechanism correlation effects are fully incorporated in the model calculations.

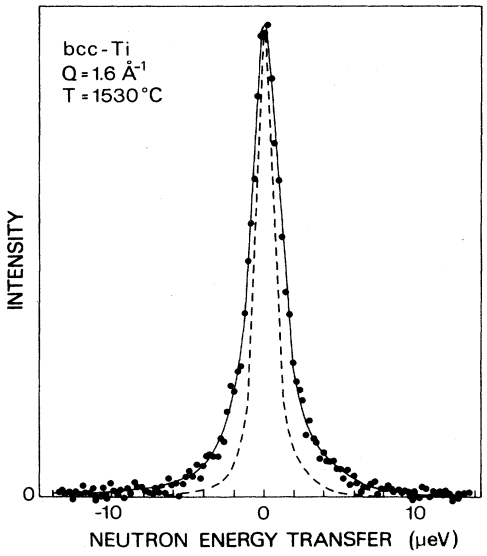

FIG. 2. Typical IN10 spectrum from single crystalline bcc Ti, fitted by a single Lorentzian (solid line), including convolution with the measured resolution (dashed line).

Before judging on the obvious domination of the NN vacancy jumps, possible admixtures of the other models have to be discussed. Assuming a similar jump frequency for an interstitial mechanism a significant admixture of these mechanisms can be definitely excluded. Because their jump length is principally small, the calculated $\Gamma(\mathbf{Q})$ always shows a hump at *large* **Q**, which is in complete disagreement with the experiment. Of course, one could argue that the interstitial jumps are much faster. This means that their diffusional line broadening is much greater and at the given temperature out of the measuring window of ± 14 μeV of the instrument. Again, the corresponding fraction can only be small because such a broader line should have been observed at lower temperatures, which was not the case (see also next paragraph).

The situation for a possible admixture of NNN jumps to the NN jumps (beyond that, which is already included in the correlation) has to be discussed in greater detail. The jump length of NNN jumps is larger than NN jumps, thus giving rise to a hump in the calculated $\Gamma(\mathbf{Q})$ at *smaller* **Q**. For the crystal 1 (1460-°C measurement) it appears that the χ^2 value for about 25% admixture of NNN jumps to NN jumps is a little better than for the pure NN jump mechanism. That is why Flottmann *et al.*[28] have discussed the physical implications of such a combined mechanism. For increasing temperature we should expect an increase of the NNN contribution because—as discussed by Flottmann *et al.*—the most probable way in which jumps to NNN sites could be achieved are jumps via divacancies, whose concentration should increase with increasing temperature.

The more recent and more extensive measurements of crystal 2 at 1530 °C, however, show within error bars no indication for a NNN jump admixture; χ^2 became smaller (the fit being better), the smaller the NNN admixture was assumed. The situation is illustrated in Fig. 5, where the pure NN fit and a fit with a hypothetical mixture of 75% NN and 25% NNN jumps to the measured $\Gamma(\mathbf{Q})$ are compared. For crystal 2 all orientations fit best with a pure NN model. For crystal 1, the orientation with $\alpha = 15°$ fits better to a model of an admixture of NN and NNN jumps, whereas the orientation $\alpha = 37°$ favors a pure NN jump model. From all measurements together we therefore conclude that a NNN jump admixture, if existing at all, can only be of minor importance, certainly lower than 25%, 10–15 % being compatible with the experiments.

For completeness Table I contains also the figures for measurements of crystal 2 at two further temperatures $T = 1465$ and 1580 °C and at constant orientation $\alpha = 15°$.

B. Polycrystalline measurements

Measurements on polycrystalline samples on IN10 were performed at lower temperatures, in particular, to

check whether a second and faster quasielastic component exists. The results were as follows. At sufficiently high temperature the whole spectra showed a quasielastic broadening and could be perfectly well fitted with *one* broadened Lorentzian. At lower temperature, however, *no* quasielastic broadening was detected. $\Gamma(Q)$ as measured on IN10 is shown in Fig. 6 for two typical temperatures. Assuming a NN jump length $d=2.34$ Å—as justified from the results of the previous section—and a corresponding correlation factor[18] $f_{\text{nucl}}=0.64$ Eq. (4) can be fitted to the experimental data, thereby yielding the jump frequency $1/\tau$.

As already mentioned, measurements at the spin echo instrument IN11 gave access to temperatures as low as 1100 and 1165 °C. Again, the shape of the measured intermediate scattering law $S(Q,t)$ gave no indication of a second and faster decay process, in particular, $S(Q, t=0)$ was found to be one.

Via Eq. (5) and (4) and under the assumption of NN jumps and inserting the proper Q value, $1/\tau_{\text{SE}}$ can be transformed to the jump frequency $1/\tau$. All polycrystalline results are listed in Table II.

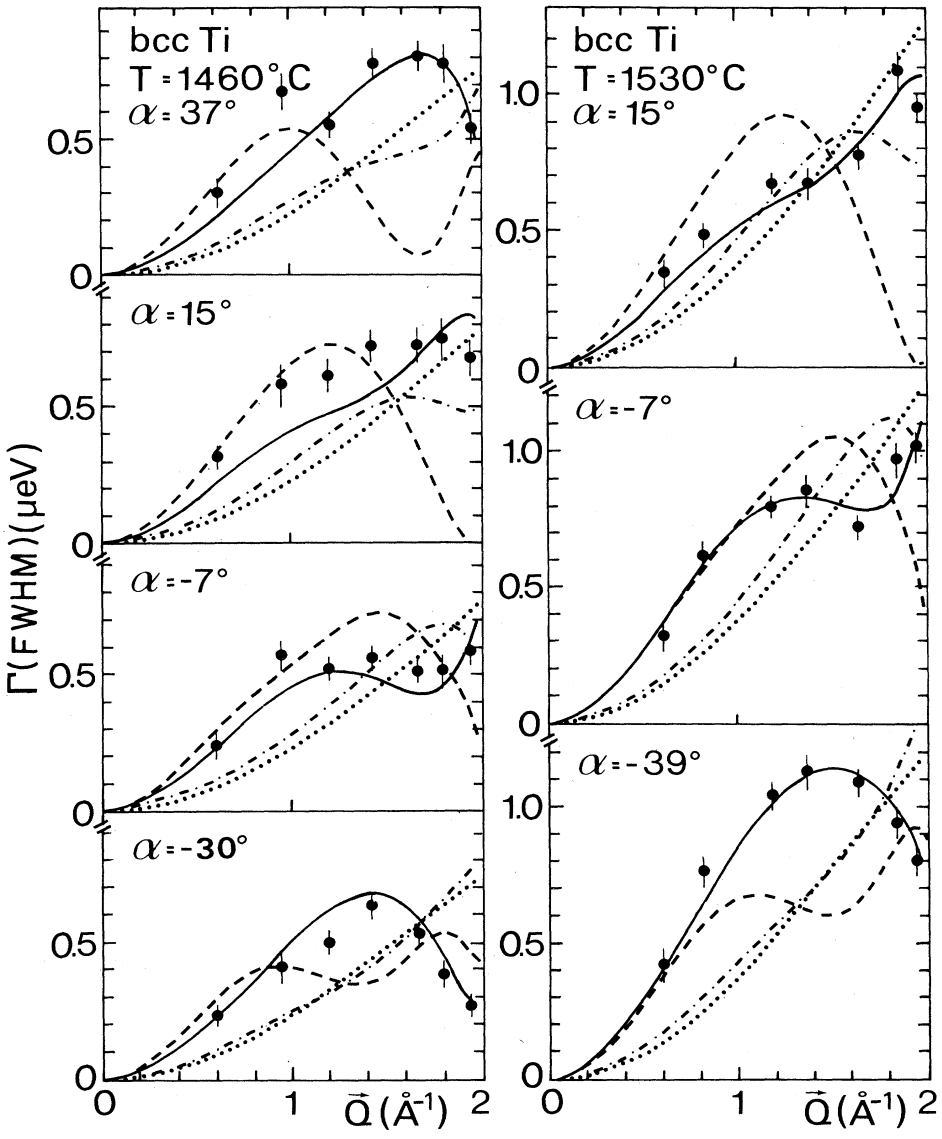

FIG. 3. Quasielastic line broadening Γ for two measuring series of bcc Ti single crystals at 1460 °C (crystal 1) and 1530 °C (crystal 2) as a function of scattering vector Q with respect to the lattice orientation. For the crystal orientation see Fig. 1. Comparison with model calculations for different diffusion mechanisms: solid line, $\frac{1}{2}[111]$ NN jumps; dashed line, [100] NNN jumps; dotted line, tetrahedral interstitial jumps; dashed-dotted line, octahedral interstitial jumps.

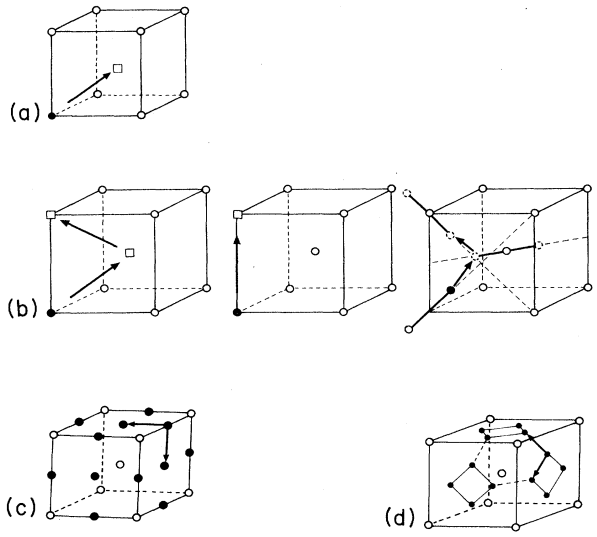

FIG. 4. Schematic representation of various diffusion jump models: (a) $\frac{1}{2}[111]$ NN jumps. (b) Three possible [100] jumps: via a divacancy, by a direct jump into a NNN monovacancy, or by three-dimensional [110] dumbbell migration. (c) Octahedral interstitial jumps, (d) tetrahedral interstitial jumps.

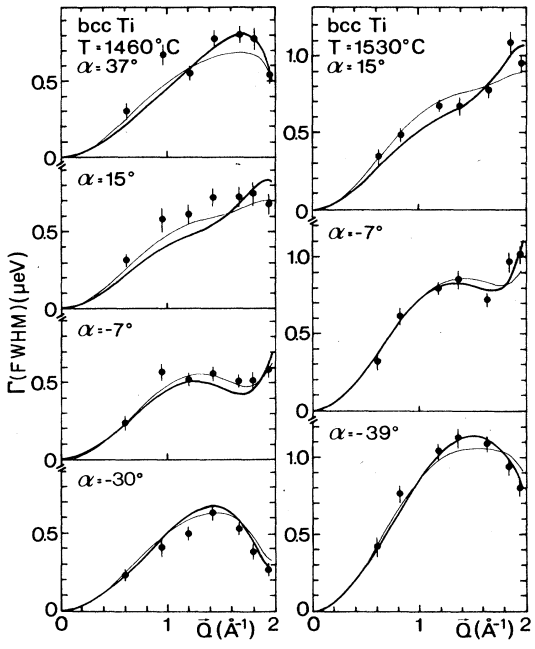

FIG. 5. Same as Fig. 3, now compared to model calculations of self-diffusion via $\frac{1}{2}[111]$ NN jumps (thick line) and self-diffusion via a mixture of 75% $\frac{1}{2}[111]$ NN jumps and 25% [100] NNN jumps (thin line). Self-correlation effects are included.

TABLE I. Parameters and results for measurements on bcc Ti single crystals.

			Crystal 1 $T=1460\,^{\circ}C$				Crystal 1 $T=1530\,^{\circ}C$				Crystal 2 $1580\,^{\circ}C$[a]				Crystal 2 $1465\,^{\circ}C$[a]			
Jump model	f_{tr}	z_{enc}	χ^2	$1/\tau$ ($10^8\,s^{-1}$)	D ($10^{-12}\,m^2\,s^{-1}$)	χ^2	$1/\tau$ ($10^8\,s^{-1}$)	D ($10^{-12}\,m^2\,s^{-1}$)	χ^2	$1/\tau$ ($10^8\,s^{-1}$)	D ($10^{-12}\,m^2\,s^{-1}$)	χ^2	$1/\tau$ ($10^8\,s^{-1}$)	D ($10^{-12}\,m^2\,s^{-1}$)				
Tetrahedral sites	1	1	21.1	8.2	1.9	33.2	13.4	3.1	20.4	16.2		4.2	7.5	
Octahedral sites	1	1	21.9	5.4	2.5	31.2	8.4	3.9	11.4	10.5		4.2	4.7	
NNN position	0.653	1.47	23.2	7.6	9.1	49.9	9.0	10.8	62.6	11.2		32.8	4.6	
NN position	0.727	1.36	2.96	5.4	5.4	1.70	8.9	8.9	7.7	9.2	9.2	0.7	4.2	4.2
75% NN plus 25% NNN			2.11	6.1	6.4	2.98	9.2	9.6	4.2	10.5		1.3	4.7	

[a]The single crystalline measurements at 1465 and 1580 °C were carried out at only *one* position, $\alpha=15°$. Therefore model fits to these temperatures are of less statistical significance. As a consequence only the diffusivities for the NN jump model are given.

IV. COMPARISON WITH TRACER DIFFUSION DATA

As described in Sec. I, from tracer diffusion data, conclusions on the elementary diffusion process can *only* be drawn rather *indirectly,* i.e., by comparing the diffusivities of various isotopes or studying the influence of solute concentrations. Thus the QNS data presented in this paper present the first direct access to the microscopic diffusion jump in group-IV*b* metals. However, in order to compare our data with the existing literature we have deduced from the QNS data the diffusivity, i.e., a property which is accessible to tracer diffusion measurements.

Before comparing our results with the tracer results we remind the reader that the virtue of QNS as a *microscopic* method is its ability to yield directly the diffusion jump vector $\mathbf{R}_n$ and the jump frequency $1/\tau$. In contrast, if one is interested in receiving *macroscopic* information, particularly on the amount of mass transport as characterized by the diffusivity, a *microscopic* method as QNS is not the first choice, such information being available more directly and with higher precision by the tracer method. Thus there are limits for a comparison as presented in the following paragraphs.

Tracer diffusion measurements on β-Ti have been performed by Murdock *et al.*,[23] Walsoe de Reca and Libanati,[24] Pontau and Lazarus[25] and Koehler and Herzig.[26] The tracer method data can be taken over a wider temperature region than with QNS, the latter being limited by the resolution of the spectrometer. Thus tracer data exist over the full temperature range from the α-β phase transition at 882 °C nearly up to the melting point at 1675 °C. Figure 7 compiles the diffusivities in the β phase resulting from the tracer measurements. Pontau and Lazarus have only measured at three temperatures, the resulting values agreeing satisfactorily with the extensive measurements of Murdock *et al.* and Koehler and Herzig, who interpreted their data in terms of a curvature of the Arrhenius plot. The values of Walsoe de Reca and Libanati are somewhat lower than those of Murdock

TABLE II. Parameters and results for measurements on bcc Ti polycrystals, assuming diffusion via NN vacancies. The lattice parameter of bcc Ti used for all calculations is $a = 3.317$ Å, and changes with temperatures have been ignored.

Temperature (°C)	$1/\tau$ (10^8 s^{-1})	D (10^{-12} m^{2}s^{-1})
1100	0.45	0.45
1165	0.68	0.68
1410	3.6	3.6
1470	4.8	4.8
1490	5.3	5.3
1540	5.7	5.7
1590	7.1	7.1
1590	9.8	9.8

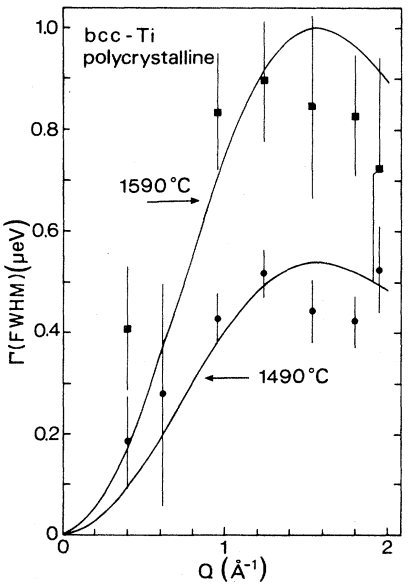

FIG. 6. Quasielastic line broadening Γ for *polycrystalline* bcc Ti at 1490 and 1590 °C as a function of the length of the scattering vector **Q**. Comparison with calculations of Eq. (4) under the assumption of diffusion via $\frac{1}{2}[111]$ NN jumps including self-correlation effects. For the fitted jump frequencies $1/\tau$ see Table II.

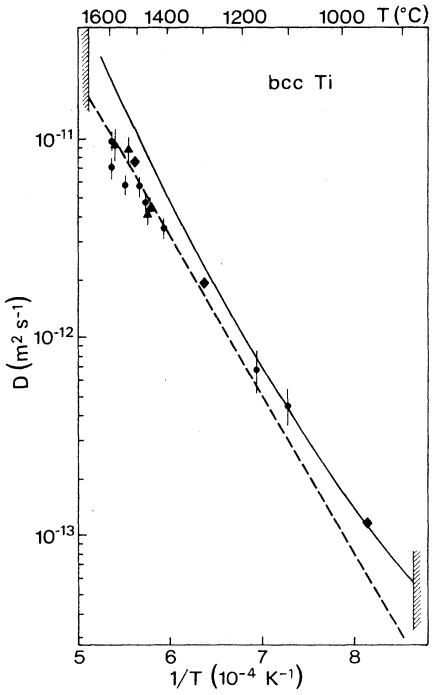

Fig. 7. Self-diffusivities for bcc Ti as deduced from the QNS measurements of the quasielastic line broadening. Compare also with Tables I and II. ▲, measurements on single crystals; ●, measurements on polycrystalline samples. Comparison with diffusivities as measured by tracer technique: ——, common fit to the data of Murdock *et al.* (Ref. 23) and Köhler and Herzig (Ref. 26); — — —, fit to the data of Walsöe de Reca and Libanati (Ref. 24); ♦, data from Pontau and Lazarus (Ref. 25).

et al. and Koehler and Herzig, and are interpreted by the authors in terms of a straight line in the Arrhenius plot. However, including the considerable error bars of Refs. 24 and 25, all measurements show a region of overlap, and the interpretation in terms of a curved Arrhenius plot is certainly more reliable.

From the QNS data we can deduce diffusivities in the following way. The Einstein-Smoluchowski equation for the diffusivity D reads in its atomistic form

$$D=\frac{1}{6}\frac{d^2}{\tau}f_{\mathrm{tr}} . \tag{6}$$

Now D can be calculated taking the values of the jump frequencies $1/\tau$ of Tables I and II. d and f_{tr} have to be chosen properly according to the diffusion model. As justified by the results of the previous section that diffusion in β-Ti is clearly dominated by NN jumps, diffusion coefficients for the polycrystalline measurements were calculated for this model only. All results are listed in Tables I and II. The diffusivities based on the NN jump model are also shown in Fig. 7.

Figure 7 shows that at high temperature the diffusivities deduced from QNS are at the lower end of the corresponding range of diffusivities, as measured by tracer technique. With the results from Table I for other diffusion mechanisms one could argue that by adding a substantial fraction of NNN jumps the diffusivities shift to higher values and to a better agreement with the tracer results. However, as discussed in the previous section, this hypothesis is incompatible with the measured Γ versus $\mathbf{Q}$.

In view of the fact that it is *not* the diffusivities at which the microscopic QNS method aims, but rather the vector and the frequency of the elementary diffusion jump, and realizing in this context that the fit quality is limited by the maximum available measuring time at the neutron spectrometer, we may regard the agreement of the diffusivities deduced from QNS on the basis of the NN model with the tracer diffusivities as satisfactory.

V. CONCLUSION

The Q dependence of the quasielastic line broadening measured in β-Ti single crystals clearly reveals that self-diffusion in β-Ti is dominated by $\frac{1}{2}[111]$ jumps into NN neighbor vacancies. Whereas we did not find any significant contribution of interstitial jumps an additional fraction of roughly 10–15 % jumps to NNN positions in the [100] direction—beyond that which is already included in the correlation effects—is compatible with the experimental results.

In view of the anomalously fast self-diffusion of β-Ti compared to that of more normal bcc metals like Cr, Mo, and W, this result is astonishing. Supposing that in the normal bcc metals self-diffusion occurs via NN vacancies, it is appealing to suggest another mechanism or at least a contribution of another mechanism to explain the anomalous self-diffusion in metals like β-Ti, β-Zr, or β-Hf. This speculation is further supported by the fact that the Arrhenius plots of the diffusivities of these metals show a strong curvature. All these suggestions are in contradiction to our findings. Our results are supported by an earlier QNS study on Na single crystals of Ait-Salem *et al.*[3] and Göltz *et al.*[4] Also these authors find NN vacancy jumps as the dominating diffusion mechanism. Concerning its diffusivity, Na lies in between the two extreme cases of Cr (rather slow) and β-Ti (fast).

Since evidently even in the extreme case of β-Ti self-diffusion occurs via NN vacancies, the following question remains: What kind of mechanism is responsible for the wide spread of diffusivities in the bcc metals? Up to now the most promising answer has been given by Köhler and Herzig,[1,9] who claim a softening of particular phonons responsible for the diffusion anomalies in the bcc metals. In particular they show that the degree of softening of the longitudinal-acoustic (LA) $\frac{2}{3}[111]$ phonon strongly correlates with the diffusion anomaly in the same bcc metal.

In a recent Letter[10] we have published first measurements of the phonon dispersion in β-Ti. Indeed, an extreme softening of the LA $\frac{2}{3}[111]$ vibrations has been observed. Because longitudinal phonons of *low frequency* and *in the [111] direction* can contribute to moving atoms in the direction of the dominating diffusion jump, it is appealing to suggest that the migration enthalpy for these jumps is considerably lowered by these (and other) soft modes.[1,9]

We therefore conclude with the following picture of self-diffusion in β-Ti (and most probably also in β-Zr and β-Hf). Diffusion is carried almost exclusively by atomic jumps into nearest-neighbor vacancies. The migration enthalpy for these jumps is considerably lowered in comparison to "normal" bcc metals due to the extreme soft phonons in the β-Ti lattice.[29]

ACKNOWLEDGMENTS

Financial support by the Bundesministerium für Forschung und Technologie, West Germany, under Project No. 03-ST1SPH-3 is gratefully acknowledged. We thank C. Herzig for discussions and advice. A. Heidemann showed us how to feed in shorter wavelength into IN10 and F. Mezei performed the IN11 measurements and had the idea how to get a magnetic-field-free furnace for high temperatures.

*Present address: AKZO Research Laboratories, D-8753 Obernburg, West Germany.

[1]C. Herzig and U. Köhler, Mater. Sci. Forum **15–18**, 301 (1987).
[2]A. De Fano and G. Jacucci, Phys. Rev. Lett. **39**, 950 (1977).
[3]M. Ait-Salem, T. Springer, A. Heidemann, and B. Alefeld, Philos. Mag. A **39**, 797 (1979).
[4]G. Göltz, A. Heidemann, H. Mehrer, A. Seeger, and D. Wolf, Philos. Mag. A **41**, 723 (1980).
[5]W. Schilling, J. Nucl. Mater. **69&70**, 465 (1978).
[6]R. W. Siegel, in *Point Defects and Defect Interactions,* edited by

J. Takamura, M. Doyama, and M. Kiritani (Tokyo University Press, Tokyo, 1983), p. 533; R. W. Siegel, J. N. Mundy, and L. C. Smedskjaer, Mater. Sci. Forum **15–18**, 451 (1987).

[7]H. I. Aaronson and P. G. Shewmon, Acta Metall. **15**, 385 (1967).

[8]J. M. Sanchez and D. DeFontaine, Phys. Rev. Lett. **35**, 227 (1975); Acta Metall. **26**, 1083 (1978); J. M. Sanchez, Philos. Mag. A **43**, 1407 (1981).

[9]U. Köhler and C. Herzig, Philos. Mag. A **58**, 769 (1988).

[10]C. Herzig and H. Eckseler, Z. Metallk. **70**, 215 (1979).

[11]W. Petry, T. Flottmann, A. Heiming, J. Trampenau, M. Alba, and G. Vogl, Phys. Rev. Lett. **61**, 722 (1988).

[12]W. Petry and G. Vogl, Mater. Sci. Forum **15–18**, 323 (1987).

[13]See, for example, T. Springer, in *Quasielastic Neutron Scattering for the Investigation of Diffusive Motions in Solids and Liquids,* Vol. 64 of *Springer Tracts in Modern Physics* (Springer, Berlin, 1972).

[14]K. S. Singwi and A. Sjölander, Phys. Rev. **119**, 863 (1960); **120**, 1093 (1960).

[15]C. T. Chudley and R. J. Elliott, Proc. Phys. Soc. London, **77**, 353 (1961).

[16]W. Petry, G. Vogl, and W. Mansel, Phys. Rev. Lett. **45**, 1862 (1980); W. Petry and G. Vogl, Z. Phys. B **45**, 207 (1982); W. Petry, G. Vogl, and W. Mansel, Z. Phys. B **46**, 319 (1982).

[17]G. Vogl, Phys. Status Solidi B **144**, 259 (1987).

[18]D. Wolf, Solid State Commun. **23**, 853 (1977); Philos. Mag. A **47**, 147 (1983).

[19]J. M. Rowe, K. Sköld, H. E. Flotow, and J. J. Rush, J. Phys. Chem. Solids **32**, 41 (1971).

[20]V. F. Sears, Chalk River Nuclear Laboratory Report No. AECL-8490, 1984 (unpublished).

[21]T. Flottmann, W. Petry, R. Serve, and G. Vogl, Nucl. Instrum. Methods **A260**, 165 (1987).

[22]W. Petry, G. Vogl, A. Heidemann, and K.-H. Steinmetz, Philos. Mag. A **55**, 183 (1987).

[23]J. F. Murdock, T. S. Lundy, and E. E. Stansbury, Acta Metall. **12**, 1033 (1964).

[24]N. E. Walsöe De Reca and C. M. Libanati, Acta Metall. **16**, 1297 (1968).

[25]A. E. Pontau and D. Lazarus, Phys. Rev. B **19**, 4027 (1979).

[26]U. Köhler and C. Herzig, Phys. Status Solidi B **144**, 243 (1987).

[27]For details how to measure directly the intermediate scattering law $S(Q,t)$, see *Neutron Spin Echo,* Vol. 128 of *Lecture Notes in Physics,* edited by F. Mezei (Springer, Berlin, 1980).

[28]T. Flottmann, W. Petry, G. Vogl, and A. Heiming, Mater. Sci. Forum **15 – 18**, 463 (1987).

[29]More details about the phonon modes and their relation to diffusion-jump mechanisms are reported by W. Petry, A. Heiming, J. Trampenau, and G. Vogl, in *Proceedings of the International Conference on Diffusion in Metals and Alloys, Balatonfüred, Hungary, 1988,* edited by F. J. Kedoes and D. L. Beke (Trans Tech, Aedermannsdorf, Switzerland, 1989).